

Mechanistic Origin and Unlocking of Negative Capacitance in Perovskites Solar Cells

Mohd Taukeer Khan,^{a,b} Peng Huang,^a Abdullah Almohammed,^b Samrana Kazim,^{a,c} Shahzada Ahmad^{a,c}

^aBCMaterials, Basque Center for Materials, Applications and Nanostructures, UPV/EHU Science Park, 48940, Leioa, Spain

^bDepartment of Physics, Faculty of Science, Islamic University of Madinah, Prince Naifbin Abdulaziz, Al Jamiah, Madinah 42351, Kingdom of Saudi Arabia

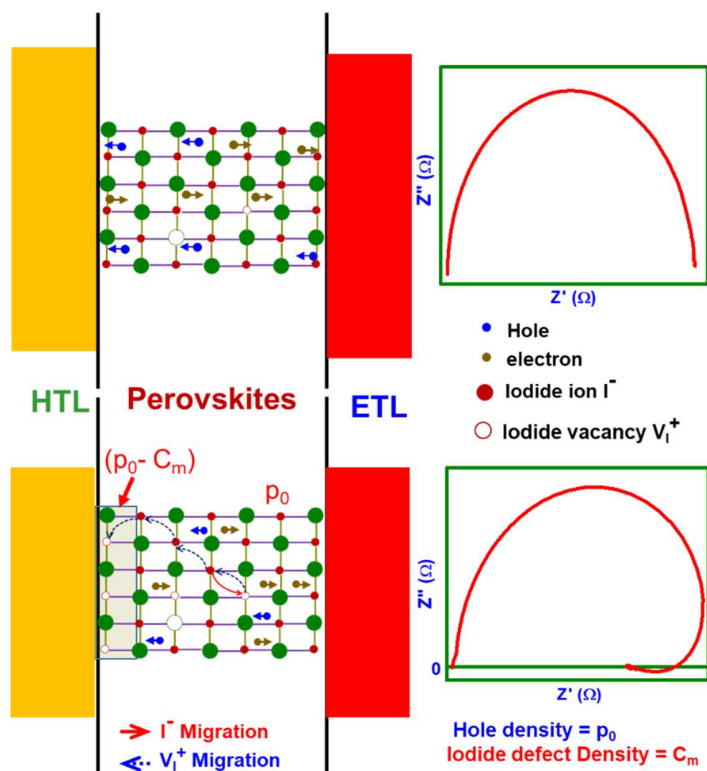
^cIKERBASQUE, Basque Foundation for Science, 48009, Bilbao, Spain

SUMMARY

Negative capacitance was found to have an adverse effect on the performance of perovskites solar cells and its origin is still under doubts. Here, we have unlocked the mechanistic behavior of negative capacitance observed at lower and intermediate frequencies by analyzing impedance spectra at variable photovoltage and applied bias, temperature dependent capacitance vs. frequency ($C-f$) spectra and current-voltage ($J-V$) characteristics. We noted inverted configuration devices having PEDOT:PSS or PTAA as hole transport layer (HTL) and PCBM as electron transport layer (ETL) exhibit the negative capacitance feature. The activation energies (E_a) for the observance of negative capacitance was found to be (394 meV and 184 meV) in similar order of magnitude required for the ionic migration. Moreover, the kinetic relaxation time (τ_{kin}) were also estimated to be $10^{-1} - 10^{-2}$ s and in the same order of magnitude required to activate the halide ion migration in perovskites solar cells. Further, beyond the activation temperature ($T_a \sim 250$ K), the trap density (n_{trap}) increases with no variation in current value signaling the creation of additional traps due to the migration of halide vacancies and recombination of charge carriers in these trap states. Subsequently, charge carrier density reduces and thus negative capacitance was observed. Our investigation suggests that the primary reason for the appearance of negative capacitance in perovskites solar cells with $p-i-n$ (inverted planar) configuration is associated with the migration of halide vacancies in the perovskites layer.

Keywords: Negative capacitance; halide vacancies; hybrid perovskite; impedance spectroscopy; defect migration; activation energy.

Graphical Abstract



HIGHLIGHTS

- Negative capacitance in inverted devices have been unraveled by immittance spectroscopy
- The migration of halide vacancies in perovskite lead to negative capacitance
- Activation energies and kinetic relaxation time of negative capacitance are in similar order of magnitude with halide ionic migration

INTRODUCTION

Despite the exceptional power conversion efficiency shown by perovskites solar cells (PSCs), they are known to suffer from a number of eccentric behaviors such as dynamic $J-V$ hysteresis,¹ giant low frequency capacitance,² inductive loop or negative capacitance etc³, and the origin of these phenomenon are still not fully understood. The negative capacitance is an ambiguous feature observed in the PSCs, have deleterious effect on device performance in terms of reduced open circuit voltage (V_{oc}) and fill factor (FF), thus yield reduced power conversion efficiency (PCE).⁴ The observance of inductive loop or negative capacitance at low and medium frequencies was explained via both bulk and interfacial effects including, ion migration and accumulation at the perovskites/charge extraction layer interface,⁵⁻⁷ trapping/detrapping of charge carriers at interfacial trap states,⁸ frequency-induced changes in resistance,⁹ and electrochemical reaction.¹⁰ Additionally, the negative capacitance was also explicated through interfacial phenomenon where the charge injection from perovskite to charge selective contact is mediated through interfacial states.^{11,12} Under open circuit conditions or due to photovoltage, the interfacial states become depopulated leading to negative capacitance.

The capacitance refers to the charge held by an arrangement for an applied voltage, accordingly, negative capacitance corresponds to the drop in stored charges, on the applied voltage increases. Recently, Ebadi et al. reported that negative capacitance is not related to classical capacitive effect and rather corresponds to slow transients in the injection current.³ Alvarez et al. found that the negative capacitance and inverted $J-V$ hysteresis in PSCs features stemmed from the same origin *i.e.* large kinetic relaxation times because of an increased recombination value.¹³ The correlation for the ionic-to-electronic current amplification for the observance of low frequency photoinduced capacitance was established,¹⁴ while the origin of the negative capacitance through the formation of an inversion layer at interface leading to over bending of energy band under illumination or open-circuit condition are also reported.¹⁵ The surface polarization model, which describes the anomalous $J-V$ hysteresis was also employed to expound the negative capacitance in PSCs. In this model, negative capacitance was assigned to the assumption of large charge accumulation at the perovskites/electron transport layer (ETL) interface which delay surface voltage, and subsequently detection of negative capacitance.^{13, 16} Inductive loop or negative capacitance are not limited to specific device configuration and reported for both type of devices ($n-i-p$ or $p-i-n$),^{3,11} with or without charge selective contacts,¹⁴⁻¹⁶ moreover

it was also noted in MAPbBr₃ single crystal.¹⁸ Thus, inductive loop and negative capacitance in PSCs are unrelated to the grain-boundary defects or interfacial phenomenon, rather it is an intrinsic property of perovskite material itself. Arguably, negative capacitance observed in PSCs is becoming one of the firmest features to interpret. So far, most of the studies on negative capacitance in PSCs are rather speculative and lack a systematic approach to elucidate its origin. Although these studies provide significant information about negative capacitance, the adequate hypothesis for its origin has not been explained yet.

In this report, we have revealed the origin of negative capacitance by investigating the bias and illumination dependence impedance spectra, temperature dependent capacitance vs. frequency ($C-f$) spectra, and current-voltage ($J-V$) characteristics. For this study, we have employed two different p-type materials (PEDOT:PSS and PTAA) in inverted configuration viz. ITO/PEDOT:PSS/PVSK/PC₆₁BM/BCP/Ag (device A) and ITO/PTAA/PVSK/PC₆₁BM/BCP/Ag (device B). The perovskite composition was kept similar for all the cases $\{(\text{FAPbI}_3)_{0.97}(\text{MAPbBr}_3)_{0.03}\}$. It was found that negative capacitance appears under the applied bias condition or above a critical temperature in both devices. Our investigation suggests that the origin of negative capacitance is related to the migration of halide vacancies due to their low activation energies.

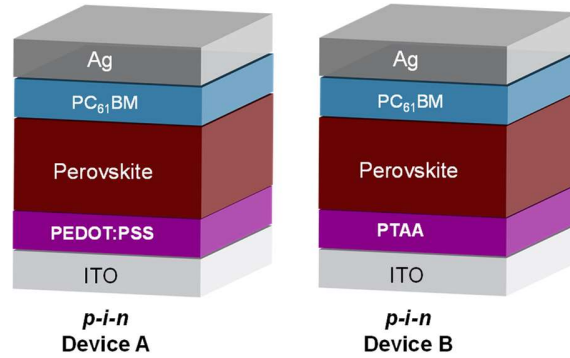


Figure 1. Schematic diagram, $p-i-n$ devices with PEDOT:PSS and PTAA as a HTM (type A and type B).

RESULTS AND DISCUSSIONS

Observance of inductive loop in impedance spectra

The impedance spectra of fabricated devices were measured at short circuit condition and in the presence of applied bias under dark and at variable illumination intensity (Figure 2). With the increase in illumination intensity, the diameter of Nyquist plot decreases. Impedance spectra in dark at short circuit conditions display a single arc, while under illumination an additional arc appears. The diameter of the left semicircle (high frequency) decreases whereas it increases for the right arc (low frequency) with the increase in illumination intensity. The high frequency semicircle described the charge transfer and recombination through perovskite/charge selective contacts while low frequency arc attributed to charge carrier ($e-h$) recombination, dielectric relaxation, and ionic migration in perovskite layer. In the presence of applied bias, the low frequency arc in both devices collapsed below the real impedance axis, drawing an inductive loop.

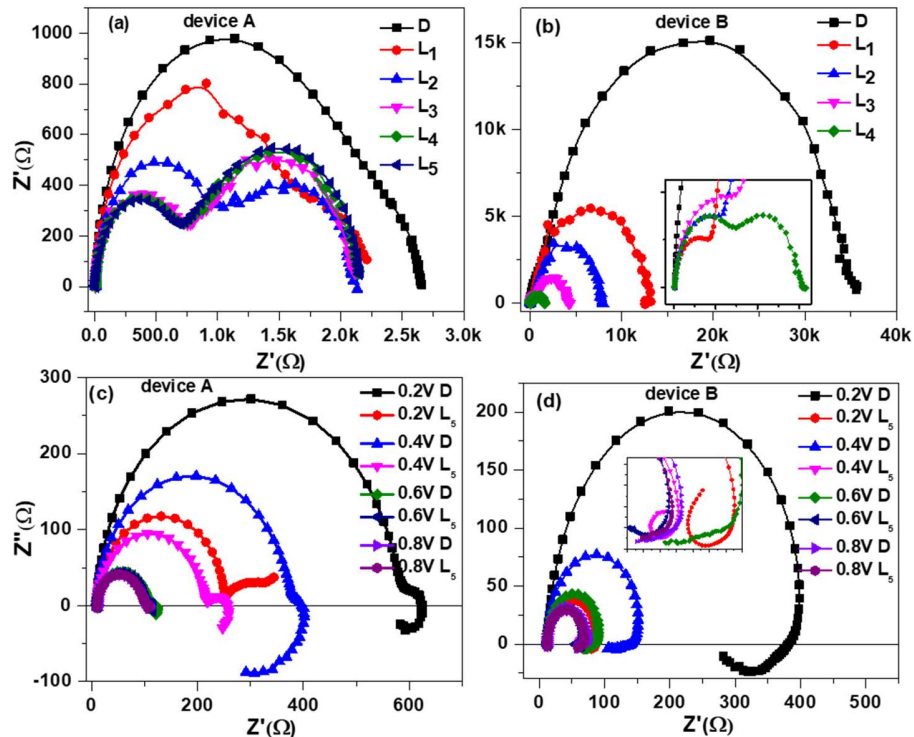


Figure 2. Impedance spectra at short circuit condition, (a-b) and at different applied bias (c-d) for type A, and type B devices. Here “D” stands for dark and “L₁, L₂, L₃, L₄, and L₅” represents the illumination intensities of 0.1, 0.2, 0.3, 0.4, and 0.5 sun, respectively.

To analyze the impedance spectra (IS), numerous equivalent circuits (EC) were used. We noted that at short circuit condition and in the presence of external field, the IS fits using EC shown in Figure S1a and S1b, respectively, and the fitting parameters are represented in Table S1, and S2 for type A, and type B devices, respectively. Here, R_s is the series resistance attributed to contacts and was in the range of 7 -12 Ω , indicating intimate device contacts. The first capacitance, C_{bulk} represents the geometrical or bulk capacitance of perovskite layer, which together with R_l accounts for the arc at high frequencies.^{10, 19} This bulk capacitance (C_{bulk}) was extracted to be of the order of 10^{-8} F, and small increment under illumination was noted, possibly due to photogeneration of charge carriers. The value of resistance R_l decrease with illumination or under applied bias due to increase in charge carrier density. The second capacitance, C_{acc} labels the ionic migration and accumulation at perovskite/ETL interface under short circuit condition and in the presence of external fields, respectively. The C_{acc} together with R_2 (related with recombination resistance), accounts for the low frequency arc.^{14,20} Ionic capacitance value in type A, and B devices under short circuit condition and dark were extracted to be 8.76×10^{-7} F, and 3.92×10^{-8} F, respectively, this value increase by an order of magnitude under light illumination. Under external bias, the accumulation capacitance further increases by an order of magnitude with respective values of 1.67×10^{-5} F and 1.99×10^{-4} F. This implies that under external bias or illumination, the ionic accumulation at the interface is higher as compared to the short circuit and dark condition. The interfacial charge transfer resistance R_2 define arc radius of inductive loop. It decreases in the presence of external fields and under illumination. According to surface polarization model, the inductance becomes prominent for larger values of the kinetic relaxation constant $\tau_{kin} = L / R_L$ (L is inductance and R_L is the resistance parallel to L), the loop becomes bigger and crosses the axis entering negative values.¹⁶ The Kinetic relaxation time for type A and B device was calculated to be 0.57 s and 2.67×10^{-2} s, respectively, which is of the same order of magnitude required for the diffusion of halide vacancies.²¹ Arguably, the diffusion of halide vacancy is one of the primary cause for the appearance of low frequency inductive loop in inverted PSCs.

Observation of negative capacitance

Mostly, inductance is related to the magnetic field which is not the case here (neither magnetic field was applied nor any magnetic material been employed). Typically, inductive loop and negative capacitance are noted in same device, therefore, inductance is considered as the effect of

reciprocal of negative capacitance. To investigate the origin of the inductive loop in impedance spectra, we made temperature dependence capacitance vs. frequency (C - f) measurements (Figure 3). The C - f spectra shows three distinct regions in agreement with previous report.²⁶ The high frequency capacitance corresponds to the series resistance of contact electrodes, the capacitance in the intermediate frequency range is related to the dielectric relaxation in the perovskite layer and determined by the geometrical capacitance per unit area. The low frequency capacitance in type A and B devices first increase exponentially and subsequently drops rapidly to below zero with negative value of capacitance. Moreover, with the increase in temperature the onset of drop frequency increases in both devices (A & B) and shifts to intermediates frequency. The rise of low frequency capacitance corresponds to charge accumulation at perovskites/HTL interface and the drop in capacitance to negative value at lower frequency corresponds to discharge of interfacial accumulated charge to the defect states due to ionic migration. With an increase in temperature, ions start to migrate faster and leave behind the trap states. The shift (increase) in drop frequency with temperature is attributed to faster (decrease) recombination $\left(\tau = \frac{1}{f}\right)$ of charge carriers in defect states created by ionic migration.

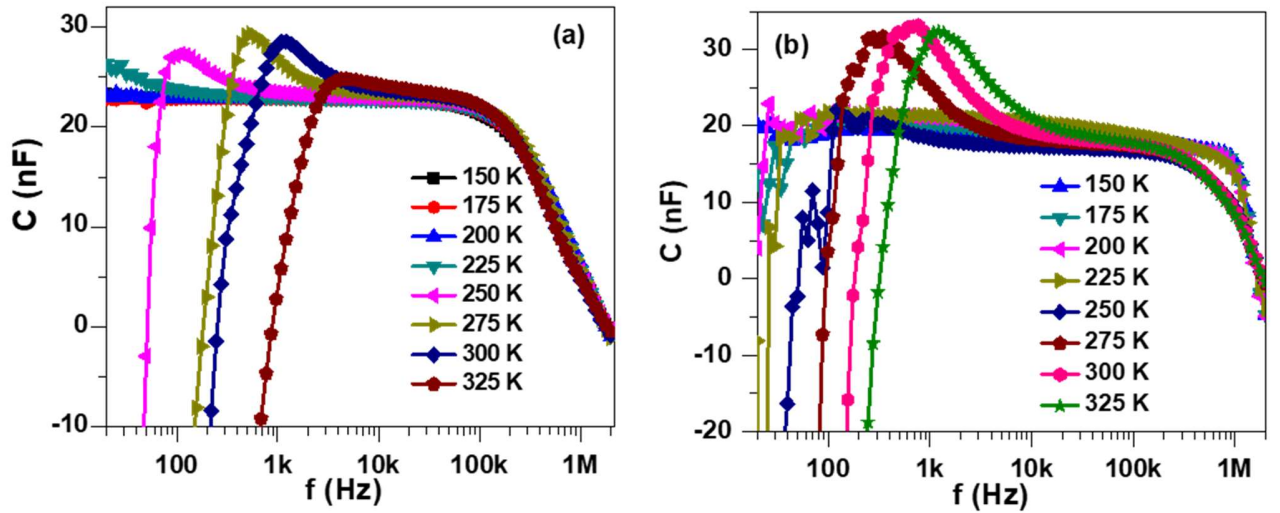


Figure 3. Capacitance vs. frequency spectra as a function of temperature (a) type A and (b) type B device.

Evidence of halide vacancy migration

The kinetic relaxation time derived for type A and B devices are in the similar order required for the diffusion of halide vacancies. To further unravel the evidence for the ionic migration in

perovskites layer, the activation energy (E_a) was calculated from the Arrhenius plot of peak frequencies (f_{peak}) [extracted from $-\ln(f \frac{dC}{df})$ vs f plot and vs. $1000/T$ (Figure 4). The activation energy for type A and B devices were calculated to be 0.39 eV, and 0.18 eV, respectively. The activation energies are in the range of the activation barrier for the migration of I^- ions (0.08 eV - 0.58 eV) and lower than the activation energies required for the migration of MA^+ ions (0.46 eV - 0.84 eV) and Pb^{2+} ions (0.80 eV - 2.31 eV).^{24, 36, 37} Owing to low activation energy, the majority of mobile ions in perovskites are suggested to be the I^- ions, which can migrate easily across the perovskite layer under external bias or with temperature rise in PSCs. This will lead to a change in local stoichiometry of the entire layer, which in turn can influence the charge transport and its characteristic resistance. The activation energy depends on a number of factors e.g. migration path (grain or bulk), grain boundaries, crystallinity and defects etc. The different activation energy in two configurations might be due to variation in perovskites structure and interfacial properties of perovskites with PTAA and PEDOT:PSS. As hydrophobic surface of PTAA is favorable for the growth of compact, pin-hole free with larger grain perovskites layers.^[38] On the other hand hydrophilic surface of PEDOT:PSS produces smaller grains and deep traps as compared to PTAA. The large size grains in perovskites layers over PTAA provide a network for the ionic migration as compared to perovskites grown atop of PEDOT:PSS. We speculate this is responsible for the lower ionic activation barrier in PTAA as compared to PEDOT:PSS.

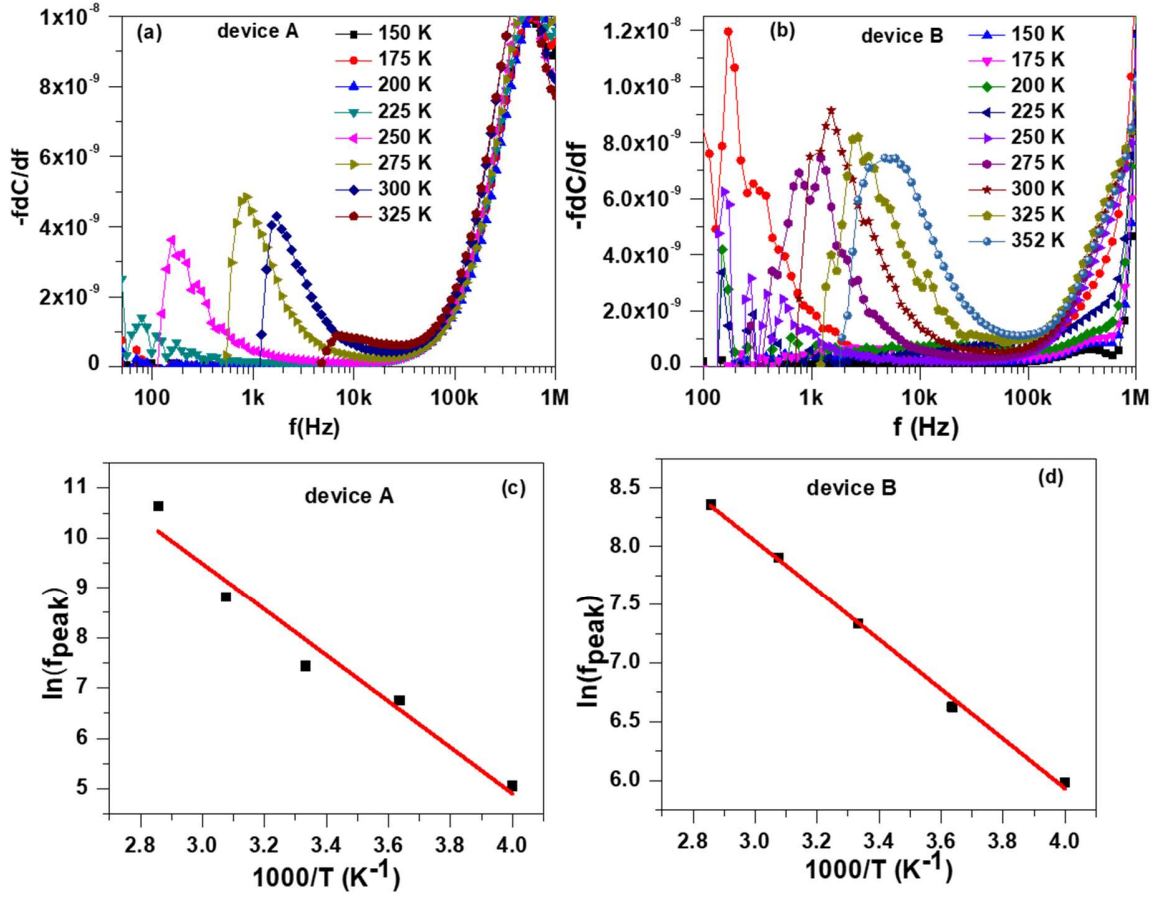


Figure 4. $(-f \times dC/df)$ vs. frequency at different temperatures for (a) Type A, (b) Type B. Arrhenius plot of peak frequency (f_{peak}) vs $100/T$ for (c) Type A and (d) Type B.

DISCUSSION

The migration rate of halide ions was evaluated through the equation: $k = \left(\frac{k_B T}{\hbar} \right) e^{-E_a/RT}$, where K_B is Boltzmann constant, T is temperature, $\hbar = h/2\pi$ is Planck constant, R is ideal gas constant and E_a is activation energy. The halide migration rate was in the order of $\sim 10^{13} \text{ s}^{-1}$ at room temperature. The low activation energy led to migration of iodide ions towards ETL with a migration rate of 10^{13} s^{-1} at room temperature. The I^- ions migration leave behind iodide vacancy (V_{I}^+) and lattice distortion due to unbalanced charge. Under the influence of external bias, these defects and iodide vacancy (V_{I}^+) migrate towards hole transport layer (HTL) and accumulate at HTL/perovskites interface (Figure 5a) with a concentration of C_m . The accumulated vacancies create shallow traps at HTL/perovskite interface, electrons from the conduction band can discharge

in these defects, and charge carrier density at interface decreases to $(p_0 - C_m)$, where p_0 is the charge carrier density in bulk of films. Thus, with an increase in external bias, the net interfacial charge decreases, resulting in observation of negative capacitance: $C = \frac{dQ}{dV}$. Our findings suggest that migration of halide ions and accumulation of halide vacancies at perovskite/HTL interface are the key reason for the appearance of negative capacitance in PSCs.

Further, the negative capacitance in type B device starts appearing at lower temperature compared to type A device (Figure 3), this is due to the activation energy in type B device is about half as compared to type A device. Thus, the migration of halide vacancies in type B device was easy as compared to type A device, consequently negative capacitance in type B device appears at lower temperature than of type A device.

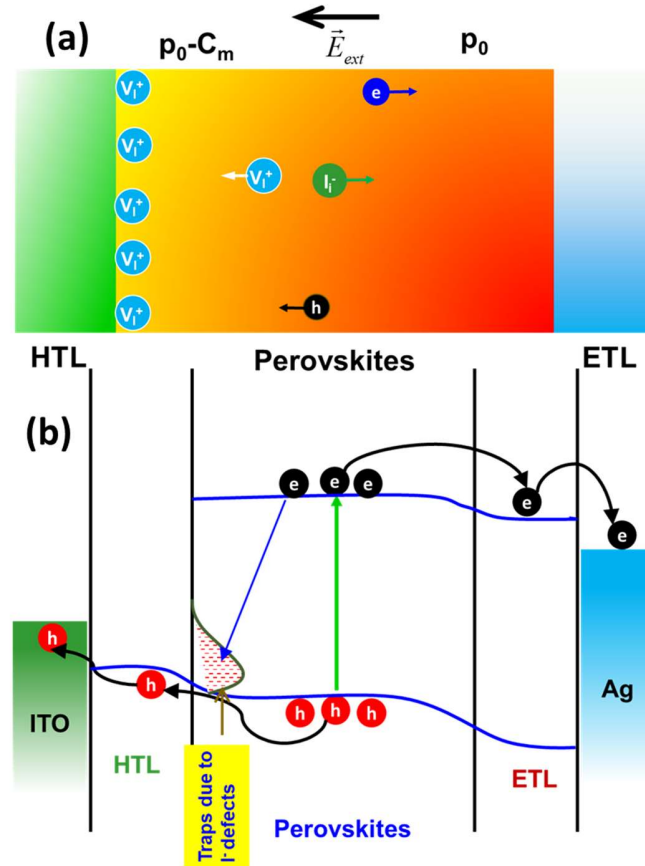


Figure 5. a) Schematic illustration of migration of iodide ions and vacancies migration in a perovskites layer under the external bias. The applied field caused diffusion of halide defects towards HTL, and compensate the iodide interstitial (I_i^-) also accumulate at HTL/perovskites interface and b) the accumulated halide vacancies creates shallow traps, where electrons recombines and reduces the interfacial charge density.

At short circuit condition, these defects follow a random migration path and distribute uniformly over the perovskite layer. At an applied bias, halide vacancies migrate towards interface of HTL/perovskites and accumulate, thus effecting the interfacial space charge region due to Fermi level equilibration.²⁶ Moreover, these defects are also thermally activated, with an increase in temperature they accumulate at interface, affecting the interfacial space charge region. To elucidate the effect of accumulation of iodide vacancies on interfacial space charge, we measured the temperature dependence dark J - V characteristics of type A and B devices (Figure 6a and 6b).

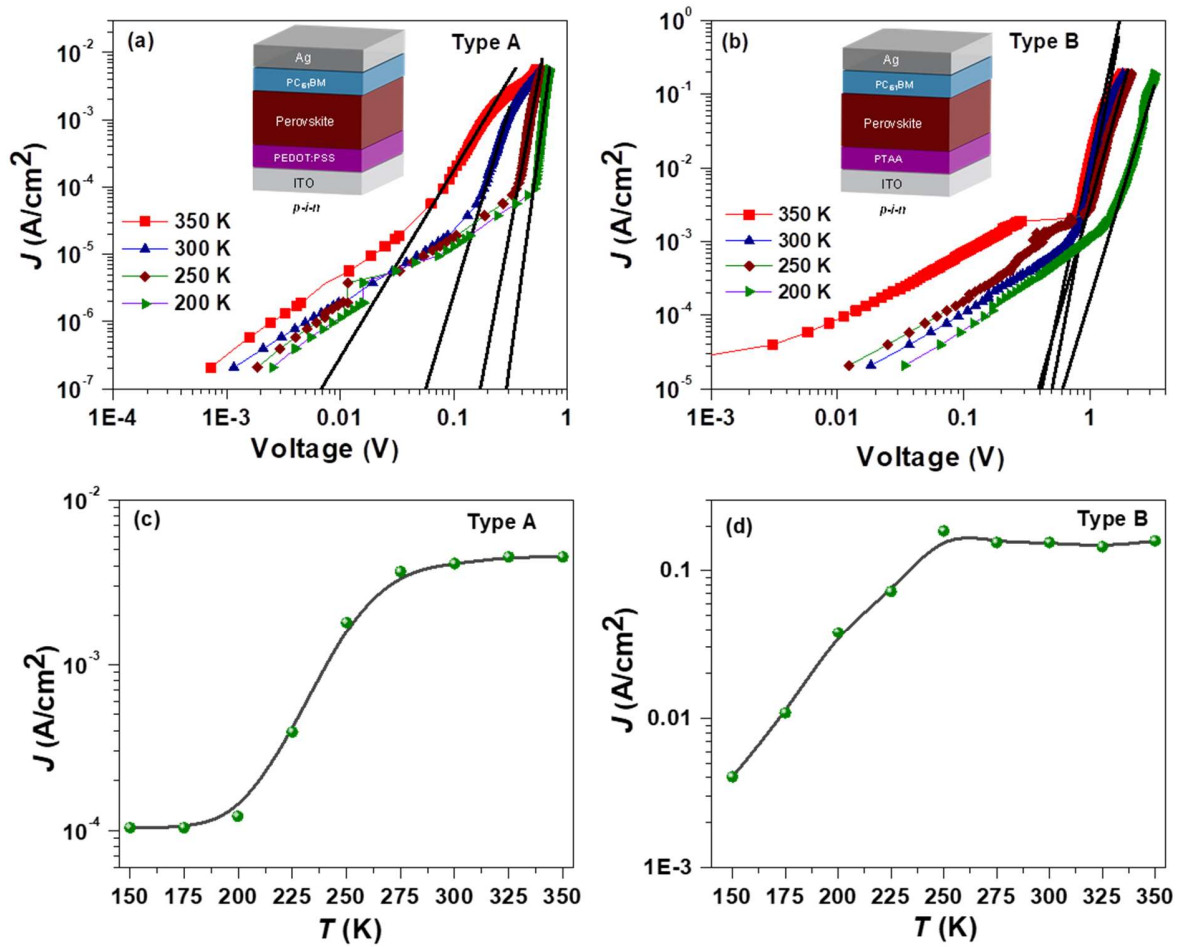


Figure 6. Experimental (symbols) and calculated (solid lines) J - V characteristics of (a) type A and (b) type B devices. Variation of current density as a function of temperature for (c) type A (at 0.5 V) and (d) type B (at 1.7 V) device.

The J - V characteristics can be divided in two regions i) lower field and ii) higher field. At low applied bias, J - V characteristics follow Ohm's law and electrical conductivity at room temperature

was evaluated to be 7.68×10^{-9} and 4.27×10^{-8} S/cm for type A and B devices, respectively. The higher conductivity in type B device has an origin due to surface properties of PTAA, that favors compact, pin-hole free devices and large grains of perovskites as compared to PEDOT:PSS.^[38] This is in accordance with the device performance (Figure S2) owing to improved efficient carrier transport.²⁷ The high field region was fitted with space charge limited current (SCLC) equation for the distribution of exponential traps:²⁸⁻³⁰

$$J = q^{1-l} \mu_{eff} N_{eff} \left(\frac{2l+1}{l+1} \right)^{l+1} \left(\frac{l}{l+1} \frac{\epsilon}{H_{eff}} \right)^l \frac{V^{l+1}}{d^{2l+1}}$$

Where, q is the total charge, N_{eff} is the effective density of states, ϵ is the permittivity of perovskite layer, d is the thickness of perovskite layer, H_{ee} is the sum of shallow density of traps at the edge of valence band and conduction band. μ_{eff} is the effective carrier mobility given by [39]:

$$\mu_{eff} = \frac{\mu_e \mu_p}{\epsilon \langle v \sigma \rangle} \frac{[B(\alpha / \beta v_{an}, \alpha / \beta v_{ap})]^3}{[B(3\alpha / 2\beta v_{an}, 3\alpha / 2\beta v_{ap})]^2}$$

Where, μ_p and μ_e hole and electron mobilities, respectively, $B(m, n)$ is the β function. σ is the capture cross section, v is thermal velocity, and the product $v\sigma$ is charge carrier capture rate constants or recombination rate constant. The fitting parameters used for type A (type B) device are: $H_{eff} = 1.3 \times 10^{16} \text{ cm}^{-3}$ ($2.90 \times 10^{16} \text{ cm}^{-3}$), $N_{eff} = 6.0 \times 10^{17} \text{ cm}^{-3}$ ($6.0 \times 10^{17} \text{ cm}^{-3}$), $\mu = 4 \times 10^{-4} \text{ cm}^2 \text{ V}^{-1} \text{ s}^{-1}$ ($5.5 \times 10^{-4} \text{ cm}^2 \text{ V}^{-1} \text{ s}^{-1}$). The effective carrier mobility in type B device was noted to be slightly higher than of type A device, a feature which is align with larger grain size in type B device. The free carrier concentration in perovskite layers was estimated to be $1.25 \times 10^{14} \text{ cm}^{-3}$ and $5.59 \times 10^{14} \text{ cm}^{-3}$ for type A and B device, respectively.

Figure 6c and 6d illustrates the variation in the current density at constant voltage at variable temperatures. It can be noted from Figure 6c and 6d that the rate of current density increase below the critical temperature is very low and it is almost constant above the critical temperature. This implies that when temperature reaches to a critical temperature, the halide defect starts migrating towards HTL/perovskites interface and the accumulation of these halide vacancies at interface rises, subsequently accumulation of capacitance increases (Figure 3a and 3b). Moreover, Minns et al. reported similar temperature (280 K) for the migration of iodide defects in MAPbI_3 via interstitial sites which is comparable to the present work ($>250 \text{ K}$).³¹ Further, we performed Mott-

Schottky analysis to derived information about the HTL/perovskites interface (Figure S3). We noted that the depletion capacitance is not clearly visible in both devices, suggesting that at room temperature the contribution of capacitance due to accumulation of halide vacancies dominates depletion capacitance in type A and B devices.³² We speculate, as the device temperature reached to critical temperature, iodide vacancies activates and migrates towards HTL, creating additional trap states [Figure 5]. Trap density (n_{trap}) increase above critical temperature can be established from the plot of variation of trap density vs. temperature (Figure S4). It can be deduced from the figures that the rate of trap density with respect to temperature starts increasing above critical temperature suggesting the increase of trap density beyond critical temperature. In case, where temperature of devices cross the critical temperature, migration of iodide vacancies is activated, leading to increase of trap density at HTL/perovskites interface (Figure 5b). The charge carriers discharged in these defect states resulted in no further increase in current (Figure 6c and 6d). Due to recombination of charge carriers in iodide recombination centers, the interfacial charge carrier density decreases which lead to the appearance of negative capacitance.

An alternative explanation for the appearance of negative capacitance can be assigned to the decrease of interfacial barrier. When the concentration of iodide vacancies (positive charge) at interface reaches to threshold, interfacial electric field increases, reduce the barrier height, which results in excess of charge carriers transfer from perovskites to HTL either via tunneling or injection as a results of increase of device current in this temperature range as shown in Figure 6c and 6d. Subsequently, interfacial charge carrier density decreases³⁴ because of negative capacitance. The origin of negative capacitance remains the same *i.e.* the migration of halide vacancy in perovskites layer and accumulation at HTL/perovskites interface.

Conclusion

To summarize, we have unraveled that under applied bias, accumulation capacitance increases suggesting accumulation of iodide vacancies at HTL/perovskite interface. We assign the origin of negative capacitance in perovskites solar cells due to the migration of halide vacancies. The inductive loop observed on the applied external bias is required to migrate the iodine vacancies. We noted similar kinetic relaxation time for the diffusion of iodine vacancies and the activation energies while activation temperature are also in the same order required for the migration of iodine vacancies. Above the activation temperature, trap density increases, the value of current becomes constant, signaling creation of additional traps due to iodine vacancies and recombination

of charge carriers in these trap states. Our findings suggest that under the activation condition, the halide defects migrate towards hole transport layers and accumulate at the interface of perovskite, charge carriers recombine in these trap states decreases carrier density, which in turn allows the appearance of negative capacitance.

3. Experimental methods

Solar cell device fabrication

For fabricating *p-i-n* (type A and B) devices, the pre-cleaned ITO substrates were treated by UV ozone for 30 min. The PEDOT:PSS as HTM layer were prepared by spin-coating from filtered PEDOT:PSS (Clevios PVP Al 4083) solution at 5000 rpm for 30 s in air, and ITO/PEDOT:PSS films were post-heated at 150 °C for 15 min and transferred into glovebox for further use. The PTAA as HTM layer was spin-coated from precursor solution (5 mg/mL PTAA in toluene) onto the ITO substrate at 5000 rpm for 30 s, and the substrates were annealed at 100 °C for 5 min in the glovebox. The perovskite layers were deposited through two-step method³⁵. Firstly, 1.3 M PbI₂ was dissolved in 1 mL of DMF and DMSO (volume ratio = 9.5:0.5) solution at 70 °C overnight. The solution was spin-coated on the ITO/HTM at 2000 rpm for 20 s, then 60 µL of the mixed solution of FAI: MABr : MACl (60 : 10 : 10 mg in 1 mL IPA) was spin-coated on the PbI₂ substrate at 2000 rpm for 20 s. The as-prepared samples were annealed at 150 °C for 15 min under 30–40% relative humidity conditions. A thin layer of PC₆₁BM (10 mg/mL in chloroform) was spin-coated on perovskite at 1500 rpm for 30 s. BCP was used as buffer layer atop of PC₆₁BM and was spun-coated from the corresponding solution (0.5 mg/mL) at 5000 rpm for 30 s. Ag electrode (100 nm) was thermally evaporated under a pressure of 4×10^{-6} Pa.

Device characterization

The current-voltage characteristics of the PSC were performed under AM 1.5G (100 mW cm⁻²) illumination that was provided by 3A grade solar simulator (Newport). The impedance measurements were carried out in the frequency range 2 MHz - 1 Hz under the perturbation of 20 mV ac signal using Biologic SP300 Potentiostat. A white LED was used to illuminate the device and illumination intensity was controlled by a controller and the range of light intensity for different photovoltage was c.a. 0.1 – 0.5 sun illumination. To minimize the noise and external interferences, a faradaic chamber was used for sample measurements. The measured data were analyzed through Z-view software (version 3.1c) by using equivalent circuits and characteristic parameters of devices were extracted. The *C-f* measurements at different temperatures were performed on a Keysight precision LCR meter (model E4980A) in the frequency range 2 MHz – 20 Hz. The temperature dependence dark *J-V* characteristics was measured using Keithley 2400 current source and voltmeter (Keithley 2110 5 ½ Digit). Linkam heating / cooling stage (Model LTS420E-PL8) was filled with liquid nitrogen and the temperature was controlled with the help of a software. Firstly, the samples were

cooled down to 150 K and thereafter measurements were carried in heating mode in the temperature range 150 K – 350 K.

Author Contributions

M.T.K performed the experiments, analysed the data and prepared the initial draft, P.H. fabricated the devices, A.A provided assistance to MTK, S.K. performed the analysis of the data, S.A. supervised and directed the research. All authors contributed to the draft and prepared the final version.

Conflicts of interest

The authors declare no conflict of interest.

Acknowledgments

This work has received funding from the European Union H2020 Programme under European Research council Consolidator grant [MOLEMAT, 726360].

Supporting Information

Admittance spectroscopy and device PV data.

References

- (1) Snaith, H. J.; Abate, A.; Ball, J. M. ; Eperon, G. E.; Leijtens, T.; Noel, N. K.; Stranks, S. D.; Wang, J. T.-W.; Wojciechowski, K.; Zhang, W. Anomalous Hysteresis in Perovskite Solar Cells. *J. Phys. Chem. Lett.* **5**, 9, 1511–1515 (2014).
- (2) Zarazua, I.; Bisquert, J.; Garcia-Belmonte, G.; J. Light-Induced Space-Charge Accumulation Zone as Photovoltaic Mechanism in Perovskite Solar Cells. *J. Phys. Chem. Lett.* **7**, 3, 525-528 (2016).
- (3) Ebadi, F.; Taghavinia, N.; Mohammadpour, R.; Hagfeldt, A.; Tress, W. Origin of apparent light-enhanced and negative capacitance in perovskite solar cells. *Nat. Commun.* **10**, 1574 (2014).
- (4). Fabregat-Santiago, F.; Kulbak, M.; Zohar, A.; Valles-Pelarda, M.; Hodes, G.; Cahen, D.; and Mora-Sero, I. Deleterious Effect of Negative Capacitance on the Performance of Halide Perovskite Solar Cells. *ACS Energy Lett.* **2**, 9, 2007-2013 (2017).
- (5) Gonzalez-Pedro, V.; Juarez-Perez, E.J.; Arsyad, W. S.; Barea, E. M.; Fabregat-Santiago, F.; Mora-Sero, I.; Bisquert, J. General Working Principles of CH₃NH₃PbX₃ Perovskite Solar Cells. *Nano Lett.* **14**, 2, 888–893 (2014).
- (6) Dualeh, A.; Tétreault, N.; Teuscher, J.; Gao, P.; Nazeeruddin, M. K.; Gratzel, M. Impedance Spectroscopic Analysis of Lead Iodide Perovskite-Sensitized Solid-State Solar Cells. *ACS Nano*, **8**, 1, 362–373 (2014).

- (7) Miyano, K.; Yanagida, M.; Tripathi, N.; Shirai, Y. Simple characterization of electronic processes in perovskite photovoltaic cells. *Appl. Phys. Lett.* **106**, 093903 (2015).
- (8) Zarazúa, I.; Han, G.; Boix, P. P.; Mhaisalkar, S.; Fabregat-Santiago, F.; Mora-Sero, I.; Bisquert, J.; and Garcia-Belmonte, G. Surface Recombination and Collection Efficiency in Perovskite Solar Cells from Impedance Analysis. *J. Phys. Chem. Lett.* **7**, 24, 5105–5113 (2016).
- (9) Klotz, D. Negative capacitance or inductive loop? – A general assessment of a common low frequency impedance feature. *Electrochem. commun* **98**, 58–62 (2019).
- (10) Zohar, A.; Kedem, N.; Levine, I.; Zohar, D.; Vilan, A.; Ehre, D.; Hodes, G.; and Cahen, D. Impedance Spectroscopic Indication for Solid State Electrochemical Reaction in (CH₃NH₃)PbI₃ Films. *J. Phys. Chem. Lett.* **7**, 1, 191–197 (2016).
- (11) Guerrero, A.; Garcia-Belmonte, G.; Mora-Sero, I.; Bisquert, J.; Kang, Y. S.; Jacobsson, T. J.; Correa-Baena, J.-P.; Hagfeldt, A. Properties of Contact and Bulk Impedances in Hybrid Lead Halide Perovskite Solar Cells Including Inductive Loop Elements. *J. Phys. Chem. C* **120**, 15, 8023–8032 (2016).
- (12) Bisquert, J.; Garcia-Belmonte, G.; Pitarch, A.; Bolink, H. J. Negative capacitance caused by electron injection through interfacial states in organic light-emitting diodes. *Chem. Phys. Lett.* **422**, 184-191 (2016).
- (13) Alvarez, A. O.; Arcas, R.; Aranda, C. A.; Bethencourt, L.; Mas-Marzá, E.; Fabregat-Santiago, F. Negative Capacitance and Inverted Hysteresis: Matching Features in Perovskite Solar Cells. arXiv:2005.11828 May **2020**.
- (14) Choi, W.; Song, S. W.; Han, S. G.; and Cho, K. The Origin of Photoinduced Capacitance in Perovskite Solar Cells: Beyond Ionic-to-Electronic Current Amplification. *Adv. Electron. Mater.* **6**, 2000030 (2020).
- (15) Feng, Y.; Bian, J.; Wang, M.; Wang, S.; Zhang, C.; Dong, Q.; Zhang, B.; Shi, Y. Interfacial negative capacitance in planar perovskite solar cells: An interpretation based on band theory. *Mater. Res. Bull.* **107**, 74-79 (2018).
- (16) Ghahremanirad, E.; Bou, A.; Olyae, S.; and Bisquert, J. Inductive Loop in the Impedance Response of Perovskite Solar Cells Explained by Surface Polarization Model. *J. Phys. Chem. Lett.* **8**, 7, 1402–1406 (2017).
- (17) Juarez-Perez, E. J.; Wußler, M.; Fabregat-Santiago, F.; Lakus-Wollny, K.; Mankel, E.; Mayer, T.; Jaegermann, W.; Mora-Sero, I. Role of the Selective Contacts in the Performance of Lead Halide Perovskite Solar Cells. *J. Phys. Chem. Lett.* **5**, 4, 680–685 (2014).
- (18) Kovalenko, A.; Pospisil, J.; Zmeskal, O.; Krajcovic, J.; Weiter, M. Ionic origin of a negative capacitance in lead halide perovskites. *physica status solidi (RRL) - Rapid Research Letters*, **11**, 3, 1600418 (2017).
- (19) Khan, M. T.; Almohammed, A. R. D.; Kazim, S.; Ahmad, S. Electrical methods to elucidate charge transport in hybrid perovskites thin films and devices. *Chem. Rec.* **20**, 5, 452-465 (2019).
- (20) Anaya, M.; Zhang, W.; Hames, B. C.; Li, Y.; Fabregat-Santiago, F.; Calvo, M. E.; Snaith, H. J.; Miguez, H.; Mora-Sero, I. Electron injection and scaffold effects in perovskite solar cells. *J. Mater. Chem. C* **5**, 634-644 (2017).
- (21) Wang, H.; Guerrero, A.; Bou, A.; Al-Mayouf, A. M.; Bisquert, J. Kinetic and material properties of interfaces governing slow response and long timescale phenomena in perovskite solar cells. *Energy Environ. Sci.*, **12** 2054 (2019).
- (22) Khan, M. T.; Salado, M.; Almohammed, A.; Kazim, S.; Ahmad, S. Elucidating the impact of charge selective contact in halide perovskite through impedance spectroscopy. *Adv. Mater. Interfaces* **6**, 21, 1901193 (2019).
- (23) Almora, O.; Aranda, C.; Garcia-Belmonte, G. Do Capacitance Measurements Reveal Light-Induced Bulk Dielectric Changes in Photovoltaic Perovskites? *J. Phys. Chem. C* **122**, 25, 13450-13454 (2018).
- (24) Azpiroz, J. M.; Mosconi, E.; Bisquert, J.; and De Angelis, F. Defect migration in methylammonium lead iodide and its role in perovskite solar cell operation. *Energy Environ. Sci.* **8**, 2118-2127 (2015).

- (25) Li, C.; Guerrero, A.; Huettnner, S. and Bisquert, J. *Nat Commun* **9**, 5113 (2018).
- (26) Khenkin, M. V.; Anoop, K. M.; Katz, E. A.; and Visoly-Fisher, I. Bias-dependent degradation of various solar cells: lessons for stability of perovskite photovoltaics. *Energy Environ. Sci.*, **12**, 550-558 (2019).
- (27) Khadka, D. B.; Shirai, Y.; Yanagida, M.; Ryan, J. W.; and Miyano, K. Exploring the effects of interfacial carrier transport layers on device performance and optoelectronic properties of planar perovskite solar cells. *J. Mater. Chem. C*, **5**, 8819-8827 (2017).
- (28) Blom, P. W. M., de Jong, M. J. M., & Vleggaar, J. J. M. Electron and hole transport in poly(p-phenylene vinylene) devices. *Appl. Phys. Lett.*, **68**, 23, 3308 – 3310 (1996).
- (29) Khan, M. T.; Agrawal, V.; Almohammed, A.; Gupta, V. Effect of traps on the charge transport in semiconducting polymer PCDTBT. *Solid-State Electron*, **145**, 49-53 (2018).
- (30) Kao, K. C. and Hwang, W. *Electrical Transport in Solids*, (Pergamon, Oxford, 1981).
- (31) Minns, J.L.; Zajdel, P.; Chernyshov, D.; van Beek, W. and Green, M.A. Structure and interstitial iodide migration in hybrid perovskite methylammonium lead iodide. *Nat. Commun.* **8**, 15152 (2017).
- (32) Futscher, M. H.; Lee, J. M.; McGovern, L.; Muscarella, L. A.; Wang, T.; Haider, M. I.; Ehrler, B. Quantification of ion migration in CH₃NH₃PbI₃ perovskite solar cells by transient capacitance measurements. *Mater. Horiz.* **6**, 1497-1503 (2019).
- (33) Li, C.; Guerrero, A.; Zhong, Y.; Gräser, A.; Luna, C. A. M.; Köhler, J.; Bisquert, J.; Hildner, R.; and Huettnner, S. Real Time Observation of Iodide Ion Migration in Methylammonium Lead Halide Perovskites. *Small*, **13**, 42, 1701711 (2017).
- (34) Chen, S.; Wen, X.; Sheng, R.; Huang, S.; Deng, X.; Green, M. A.; Ho-Baillie, A. Mobile Ion Induced Slow Carrier Dynamics in Organic–Inorganic Perovskite CH₃NH₃PbBr₃. *ACS Appl. Mater. Interfaces*, **8**, 8, 5351 (2016).
- (35) Huang, P.; Yuan, L.; Zhang, K.; Chen, Q.; Zhou, Y.; Song, B.; and Li, Y. Room-Temperature and Aqueous Solution-Processed Two-Dimensional TiS₂ as an Electron Transport Layer for Highly Efficient and Stable Planar n–i–p Perovskite Solar Cells. *ACS Appl. Mater. Interfaces* **10**, 17, 14796–14802 (2018).
- [36] Eames, C., Frost, J.M., Barnes, P.R., O’reagan, B.C., Walsh, A., Islam, M.S.: Ionic transport in hybrid lead iodide perovskite solar cells. *Nat. Commun.*, **6**, 7497 (2015)
- [37] Haruyama, J., Sodeyama, K., Han, L., Tateyama, Y.: First-principles study of ion diffusion in perovskite solar cell sensitizers. *J. Am. Chem. Soc.*, **137**, 10048–10051 (2015).
- [38] S. Shao, M. A. Loi, The role of the interfaces in perovskite solar cells, *Adv. Mater. Interface*, **7**, 1901469 (2020).
- [39] K. C. Kao and W. Hwang, *Electrical Transport in Solids* (Pergamon, Oxford, 1981)